Determination of Respiratory Parameters by Means of Hurst Exponents of the Respiratory Sounds and Stochastic Processing Methods

Esra Saatci and Ertugrul Saatci, *Member, IEEE*

***Abstract*—*Objectives:* System approach to the human respiratory system and input/output signals which characterize the system properties were not explored in detail in the literature. The aim of this study is to propose a combination of methods to investigate the indirect relationship between the fractal properties of Respiratory Signals (RS) and Respiratory Sound Signals (RSS) and the clinically measured respiratory parameters. *Methods:* We used Hurst exponent to reveal the fractal properties of RS and RSS and to estimate the pressures in the respiratory system. The combination of well-known statistical signal processing methods and optimization were applied to the experimentally acquired 23 records. Pearson correlation coefficient and Bland-Altman analysis were the chosen validation methods. *Results:* Considerable amounts of Hurst exponent values of RSS were found to be between 0.5 and 1, which means increasing trend or decreasing trend can be seen in RSS with fractional Gaussian process properties. Results of the pressure estimator revealed that internal pressure due to tissue viscoelasticity is higher than the pressure due to static elasticity. Feature power and skewness also provided distinctive results for all recordings. *Conclusion:* Hurst exponent values of the RSS are fruitful representation of the signals which bring the underlaying system characteristics into the surface. We illustrated that required number of sensors can be reduced in the feature calculation to ease implementation effort on the hardware of the handheld devices. *Significance:* Bland-Altman plots were very successful to demonstrate the connection between the sets of measured respiratory parameters and calculated features.**

***Index Terms*—Hurst exponent of the respiratory sound signals, respiratory parameter determination, respiratory signal processing, Bland-Altman analysis.**

I. Introduction

RESEARCHERS and practitioners studied respiratory system from different perspectives in order to differentiate the diseased conditions from the healthy conditions. If one concentrates on the system identification based on signal processing approaches, three directions of the studies, albeit connected and overlapped, can be easily distinguished. In the first direction, a major group of researchers worked with the forced oscillation technique in which oscillation response of the system was used to extract the information about the system [1]. In this respect, time domain system models (Power Law Models) [2], frequency domain system models (Constant Phase Models) [3], [4] and time domain input-output relationship models (Linear Parametric Models and Fractional Order Models) [5], [6], [7] were proposed and model parameters that were identified in experiments were calculated or estimated by fundamental signal processing methods. However, estimating the model parameters in both time and frequency domains by minimizing the selected errors or optimizing the selected criteria do not mean that system's structure will be revealed, even though the perfect model is utilized. Because the effects of the system's structure hidden in the measured signals were disregarded in the calculations.

In the second direction, while most researchers were only utilizing Respiratory Signals (RS) which are merely airflow and mouth pressure (in addition to these signals, in this study breathing air temperature and humidity are counted as RS), Respiratory Sound Signals (RSS) (including bronchial and tracheal sounds) were also integrated to the algorithms by well known methods such as the wavelet analysis [8], [9], independent component analysis [10] and adaptive filters [11] in order to classify the diseased or abnormal conditions. Although these studies grasped the power and usefulness of statistical approaches and complexity of the signals, intentions were not to elaborate the respiratory system structure and parameters.

In the third direction, RSS were processed by the methods used in complexity analysis, such as entropy and fractal analysis [12]. However, these studies were set to identify the stochastic behaviour of the signals alone, leaving out the respiratory structure and parameters.

On the other hand, fractal nature of the lungs was proved in the morphologic models, concurrently lung tissue response to the stimulus was modeled by the power law due to the viscoelastic properties [13]. However, there is only a few studies inspecting the fractal properties of the signals which are originated from the fractal and complex structured respiratory system [14]. For example, in [15] most of RS and all of RSS were proven to be multifractal signals. RS and RSS are comprehensive reflections

Manuscript received November 24, 2020; revised March 22, 2021; accepted May 5, 2021. Date of publication May 11, 2021; date of current version November 22, 2021. This work was supported in part by the Scientific and Technological Research Council of Turkey (TUBITAK), under Grant 117E721 and in part by the Research Fund of Istanbul Kultur University, under Grant IKU-BAP1801. *(Corresponding author: Esra Saatci.)*

Esra Saatci is with the Electrical and Electronics Engineering Department, Istanbul Kultur University, Istanbul 34158, Turkey (e-mail: esra.saatci@iku.edu.tr).

Ertugrul Saatci is with the Electrical and Electronics Engineering Department, Istanbul Kultur University, Turkey.

Digital Object Identifier 10.1109/TBME.2021.3079160

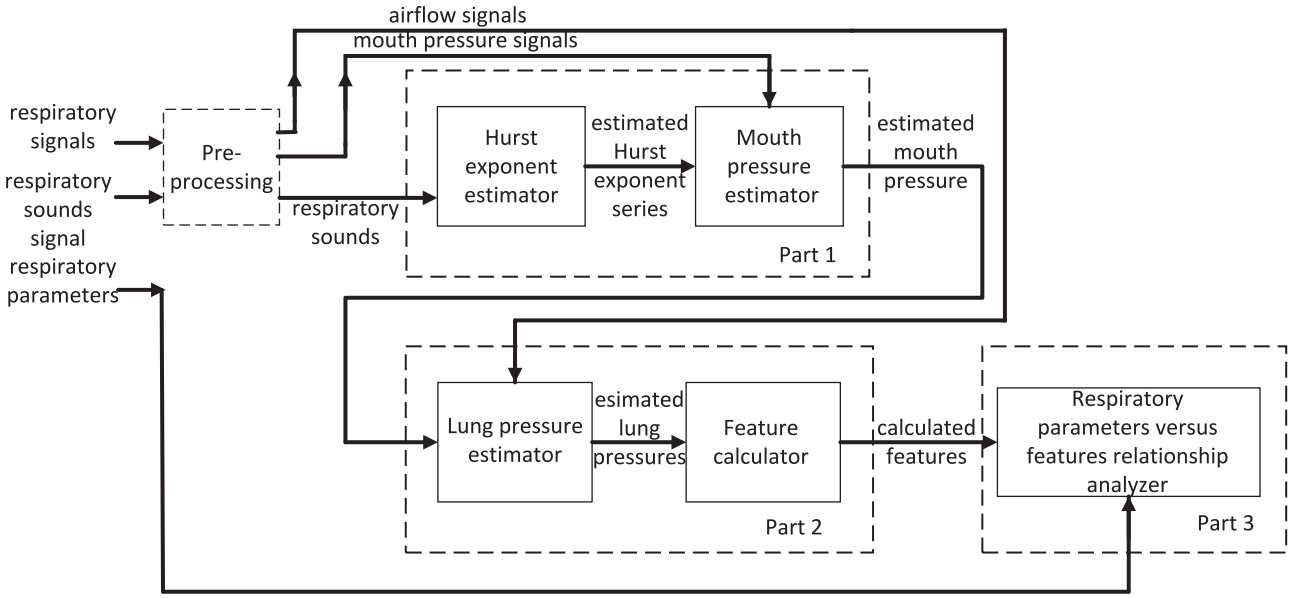

Fig. 1. Block diagram of the proposed method.

of the breathing action and the complex system structure and thus they provide a valuable information for the respiratory system analysis. In summary, since the weakest part of the previous investigations is that the intrinsic complexity and nonlinearity of the respiratory system were not elaborated adequately by the signal processing methods and not incorporated into system identification approaches, we propose to integrate fractal properties of RS and RSS (which is linked to the intrinsic complexity and nonlinearity of the respiratory system) and respiratory system identification (which is linked to the respiratory parameter estimation).

In this regard, the aim of this study is to investigate the indirect relationship between the fractal properties of RS and RSS and the clinically measured respiratory parameters. On this way, we first propose to employ Hurst exponent [16], [17], that is one of the influential parameters in the fractal analysis, which will indicate the intrinsic complexity in RSS in return. RS and RSS were already analyzed by using Hurst exponents in [15]. Hurst exponent series obtained from RSS, will be used to predict the mouth pressure with the help of the Recursive Least Squares (RLS) method. The reason for this is to eliminate the need of mouth pressure measurements in the identification of the respiratory system structure and parameters. Predicted mouth pressure will be then used to estimate internal pressures in the lung, which can not be measured non-invasively by using Kalman Filter and Optimization methods. Finally features extracted from the predicted internal pressures in the system, by the help of viscoelastic model, will be used as indicators of the respiratory parameters. At the end when we establish a link between the extracted features and the clinically measured respiratory parameters, in fact, we estimate the clinically measured respiratory parameters (not the model parameters) by combining the fractal properties of RS and RSS, traditional system models and statistical signal processing methods.

II. Methods

The proposed method is composed of three different parts consisting of a combination of estimators, feature calculator and analyzer as shown in Fig. 1. Part 1 is composed of Hurst exponent estimator and mouth pressure estimator. Local Hurst exponents are predicted by the DFA method and expressed in the form of a time series, then fed into mouth pressure estimator, by which best mean squared error is obtained with respect of window length and RSS. Part 2 contains an internal pressure estimator, in which well-known viscoelastic model with statistical signal processing methods are utilized and model parameters are estimated in the designated settings, and a feature calculator, in which features are extracted. Finally, Part 3 is for analysing the perfect matches between features and clinically measured parameters. Before going into details of the fundamental blocks and the processing algorithms functioning in the blocks, measured signal types and preprocessing should be explained.

A. Preprocessing

RS and RSS were collected from eleven healthy subjects (six male, five female) with their consent. Subjects 6 and 8 were removed from the final processing part (Part 3) due to the lack of lung function tests for the respiratory parameters. Subjects were sitting while wearing a microphone set recording lung sounds in 6 channels and tracheal sound in 1 channel, and breathing through pneumotachograph, pressure, temperature and humidity sensor set which are recorded by using another 4 channels. Fig. 2(a) shows the measurement set-up with microphones, pneumotachograph and sensor system, whereas the position of the lung sound sensors can be seen in Fig. 2(b). Subjects breathed quietly ($\sim$ 40 l/min) for 60 s and forcefully ($\sim$ 120 l/min) for 60 s and the signals were recorded via a data acquisition system with a sampling frequency of 8000 Hz. We also recorded one set

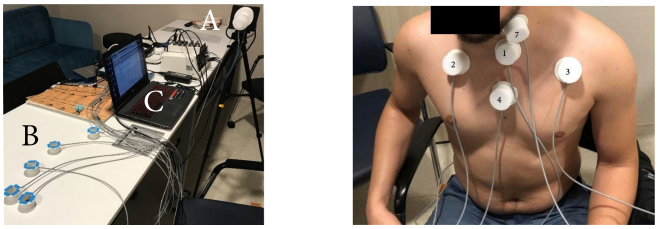

(a) (b)

Fig. 2. (a) Measurement set-up with pneumotachograph and sensor system (A), microphones (B) and data acquisition system (C), and (b) position of the lung sound sensors. Sensors 5 and 6 are at the back of the subject and cannot be seen in the picture.

TABLE I
MEASURED SIGNALS AND TESTS PARAMETERS

Channel Category	Signal	Symbol
Respiratory Signals (RS)	Airflow rate	$Q(n)$
	Mouth pressure	$P_{ao}(n)$
	Lung volume	$V(n)$
	Air Temperature	$T(n)$
	Air Humidity	$H_u(n)$
Respiratory Sound Signals (RSS)	Bronchial sounds	$LS1(n) - LS6(n)$
	Tracheal sounds	$LS7(n)$
Respiratory Parameters Spirometric Tests	Forced Expiratory Volume 1	FEV1
	Forced Vital Capacity	FVC
	Peak Expiratory Flow	PEF
Respiratory Parameters Plethysmographic Tests	Residual Volume	RV
	Total Lung Capacity	TLC
	Specific Airway Resistance	sR_{aw}
	Airway Resistance	R_{aw}
Respiratory Parameters Impulse Oscillometry Tests	Resistance at $5Hz$	R_5
	Reactance at $5Hz$	X_5
	Resistance at $35Hz$	R_{35}
	Reactance at $35Hz$	X_{35}
	Resonance Impedance	AX

of measurements belonging to Subject 2 in very high inspiratory flow rate, thus in total 23 signal sets (Recordings) were processed in the Part 1 and Part 2 but 19 signal sets (Recordings) were used in Part 3. Each period in the breaths were separated by zero-crossing method applied to airflow signals. Signals were not digitally filtered, because any filtering operation changes the signal sample values, altering the relationship between the samples. Thus RS and RSS were used as raw signals. All measurements are summarized in Table I and subjects' recordings used in blocks can be seen in the Table II.

B. Hurst Exponent Estimator

In Hurst exponent estimator we used RSS, mainly because of two reasons. First, respiratory sounds are very often analyzed in terms of intensity for the acoustical respiratory monitoring [9]. Second, measurement of RSS is fairly easy due to the microphone technology in the handheld devices such as mobile phones [12]. Moreover airflow estimation by RSS was already studied in the literature [18]. Thus, RSSs are the best candidate signals to substitute both airflow and pressure measurements in the respiratory system. In this study, we adopted Detrended Fluctuation Analysis (DFA) as proposed in [16] in order to estimate Hurst exponent, H. Algorithm 1 summarizes Hurst exponent calculation in RSS by the DFA. The detail of the algorithm can be found in the Appendix.

Hurst exponent values found by DFA are between $0 \leq H \leq 2$. If the signal has Hurst exponent between $0 \leq H \leq 1$, it has a fractional Gaussian noise (fGn) property, whereas if it is between $1 < H \leq 2$, the signal has a fractional Brownian motion (fBm) property. Statistical properties of fGn and fBm are given in [19]. Statistical evaluation of the RSS is out of scope of this study. It is important to emphasize that Hurst exponent time series are used because it reflects long memory and self similarity properties of the physical systems, which make them perfect candidate for being used to estimate the pressures in the respiratory system.

TABLE II
SUBJECTS, RECORDINGS AND METHOD PARTS CHART. ITALIC RECORDS BELONG TO HIGH FLOW RATE RECORDINGS

Subjects	Recordings	Length of 3 Periods Data Points, N	Method Parts
Subject1	Recording1	102.977	
	Recording2	96.928	
Subject2	Recording3	86.643	
	Recording4	75.352	
	Recording5	74.764	
Subject3	Recording6	164.170	Part1,2,3
	Recording7	109.788	
Subject4	Recording8	90.704	
	Recording9	68.786	
Subject5	Recording10	36.173	
	Recording11	43.506	
Subject6	Recording12	107.346	Part1,2
	Recording13	86.162	
Subject7	Recording14	50.554	Part1,2,3
	Recording15	51.054	
Subject8	Recording16	146.259	Part1,2
	Recording17	64.740	
Subject9	Recording18	92.369	
	Recording19	63.721	
Subject10	Recording20	131.005	Part1,2,3
	Recording21	119.483	
Subject11	Recording22	114.026	
	Recording23	121.308	

Algorithm 1: Hurst Exponent Estimator.

Require: $x(n), 0 \leq n \leq N-1$
Require: The set of time scale 16 *sample* (2 *ms*) $\leq s \leq N/4$
  Calculate the profile Y_i by (10)
  while 16 $sample$ (2 ms) $\leq s \leq N/4$ **do**
    Calculate the total number of segments $N_s \equiv \text{int}(N/s)$
    while $v = 1, \ldots, 2N_s$ **do**
      Compute the segments $Y_v(i)$,
      Compute local trend by mth order polynomial $y_v(i)$
      Compute and store mean squares fluctuation $F^2(v,s)$ by (11)
      $v \leftarrow v + 1$
    end while
    Compute second order fluctuation function $F_2(s)$ by (12)
    $s \leftarrow s_{new}$
  end while
  Calculate and store Hurst exponent H through logarithm function by (13)
  return Hurst exponent H

C. Mouth Pressure Estimator

Mouth pressure is estimated by using Hurst exponents time series. Before estimating the mouth pressure signals, Hurst

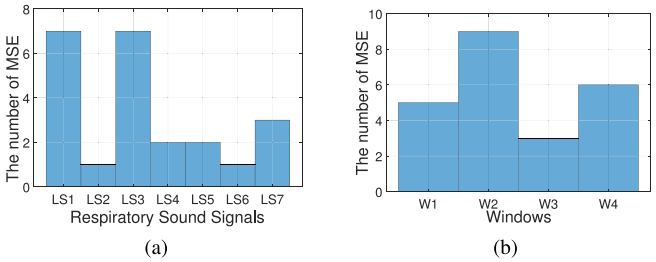

Fig. 3. The number of minimum MSE values obtained from total 23 recordings versus (a) RSS and (b) different window lengths chosen from the vector $\mathbf{W}$.

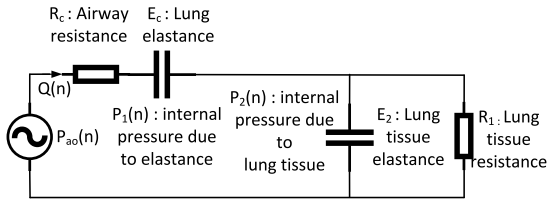

Fig. 4. Electrical analogy of the viscoelastic model.

exponents time series must be calculated. In this study, three consecutive periods of RSS (total length is N) were analyzed by non-overlapping windows with length W_{length} chosen from the vector $\mathbf{W} = [\,256\ 512\ 1024\ 2048\,]$. Thus the length of the Hurst exponents time series, $\mathbf{H}$, will be $N_{hurst} \equiv \mathrm{int}(N/W_{length})$.

Also in the study, we adopted well known Recursive Least Squares (RLS) adaptive filter as proposed in [20] for the system identification. In RLS algorithm we assumed that the order of the designed filter was 20, input and desired input were Hurst exponents time series, $\mathbf{H}$, and down-sampled mouth pressure signal $P_{ao,i}$, $1 \leq i \leq N_{hurst}$, respectively and forgetting factor was $\lambda = 0.99$. Initials were $\mathbf{a}(0) = \mathbf{0}$ for the tap weights and $\mathbf{P}(0) = 0.1\mathbf{I}_{20}$ for the covariance matrix.

However, before the estimation, we should investigate which RSS is the best suited for this method of mouth pressure estimation by Hurst exponent and determine the window length. Thus mean squared error (MSE) was calculated for all mouth pressure estimates as:

$$MSE(window, subject, RSS, channel) = \frac{1}{N_{hurst}} \sum_{i=1}^{N_{hurst}} \left(P_{ao,i} - \hat{P}_{ao,i}\right)^2 \quad (1)$$

here $P_{ao,i}$ is down-sampled $P_{ao}(n)$ and $\hat{P}_{ao,i}$ is its estimate. Fig. 3(a) shows the number of minimum MSE values obtained from total 23 recordings. As seen clearly from the figure, LS1 and LS3 were provided the highest number of minimum MSE values, which makes them best candidate for the mouth pressure estimator input. LS1 is a bronchial RSS recorded at the suprasternal notch, whereas LS3 is a bronchovesicular RSS recorded at the 1st and 2nd intercostal area, left of sternum. It is surprising that LS7, which is the tracheal RSS having the maximum intensity yielded low number of minimum MSE values in the mouth pressure estimator. Window length also affects the mouth pressure estimation. Increasing the window length, reduces the number of samples of the Hurst exponents time series and worsen the estimation. Although longer Hurst exponents time series are obtained by lower window lengths, they fail to express the statistical properties of the RSS because of the unreliably short averages. Fig. 3(b) shows the number of minimum MSE values versus window lengths chosen from the vector $\mathbf{W}$. According to the figures, $LS1$ and $W_{length} = 512$ are the best choices and thus we used LS1, window length of 512 and three consecutive periods for all RSSs in the mouth pressure estimator.

D. Lung Pressure Estimator

As a next step internal pressures in the respiratory system should be estimated. The intention here is to estimate all pressures by using mouth pressure which is previously estimated from RSS via Hurst exponents time series. Because the mathematical model needed for the estimation process, parametric respiratory system model was employed. Viscoelastic model [6] can serve greatly as the link between the respiratory pressure and airflow. Fig. 4 shows the electrical analogy of the model with model parameter explanations and dynamic properties. This model can be described mathematically by state-space equations given in (2) for $1 \leq i \leq N_{hurst}$

$$\begin{aligned} \mathbf{x}_{i+1} &= \mathbf{A}'(\theta)\,\mathbf{x}_i + \mathbf{B}'(\theta)\,\mathbf{u}_i + \mathbf{v}'_i \\ \mathbf{y}_i &= \mathbf{C}(\theta)\,\mathbf{x}_i + \mathbf{D}(\theta)\,\mathbf{u}_i + \mathbf{w}_i \end{aligned} \quad (2)$$

where $\mathbf{x}_i = [\,P_{1,i}\ P_{2,i}\,]$ is the internal pressure vector containing the states of the model, $\mathbf{y}_i = Q_i$ is called as the output signal which is the decimated airflow signal in the model and $\mathbf{u}_i = \hat{P}_{ao,i}$ is the input signal which is the estimated mouth pressure. $\mathbf{A}'(\theta) = \mathbf{I} + t_s\mathbf{A}(\theta)$, $\mathbf{B}'(\theta) = t_s\mathbf{B}(\theta)$, $\mathbf{C}(\theta)$ and $\mathbf{D}(\theta)$ are state transition, input, output and input-to-output transition matrices in discrete-time which are obtained by using matrices given in (3).

$$\mathbf{A}(\theta) = \begin{bmatrix} \frac{-E_2(R_1+R_c)}{R_1R_c} & \frac{-E_2}{R_c} \\ \frac{-E_c}{R_c} & \frac{-E_c}{R_c} \end{bmatrix} \quad \mathbf{B}(\theta) = \begin{bmatrix} \frac{-E_2}{R_c} \\ \frac{E_c}{R_c} \end{bmatrix}$$

$$\mathbf{C}(\theta) = \begin{bmatrix} \frac{-1}{R_c} & \frac{-1}{R_c} \end{bmatrix} \qquad \mathbf{D}(\theta) = \begin{bmatrix} \frac{1}{R_c} \end{bmatrix} \quad (3)$$

Initials in (2) are assumed to be zero. t_s is the sampling period. State $\mathbf{v}'_i \sim \mathrm{N}(0, \mathbf{Q})$ and measurement $\mathbf{w}_i \sim \mathrm{N}(0, \mathbf{R})$ noises are added to the state-space equations, because state and measurement trajectories in the estimations include noises with covariance matrices $\mathbf{Q}$ and $\mathbf{R}$, respectively. $\theta = [\,R_c\ R_1\ E_c\ E_2\,]$ is the model parameter vector containing model parameters which are related to the respiratory parameters. As can be seen from the system equations, system is linear in states, however nonlinear in parameters.

Both internal pressure vector and the parameter vector in (2) should be estimated at the same time. Thus we employed Kalman Filter for the estimation of the states and an optimization solver for the calculation of the optimum model parameters. Block diagram in Fig. 5 shows how Kalman filter and optimization

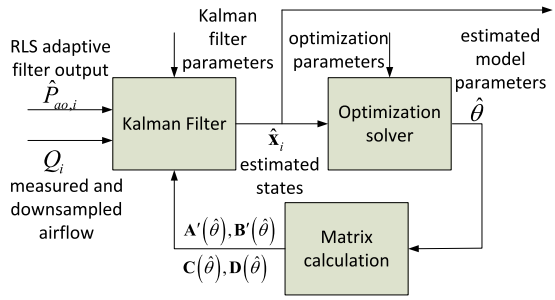

Fig. 5. Block diagram showing the estimation of internal pressures by Kalman filter and optimization solver.

solver were used in this study. The idea is to iterate Kalman filter and optimization solver in a loop until Kalman filter state error covariances drop in the Kalman iterations. We discovered that after 8th iteration, error covariance dropped to its minimum in all 23 signal sets. Kalman filter algorithm details for linear dynamic systems with Gaussian or non-Gaussian noise can be found in [21]. In the algorithm, the most important decision is the choice of covariance matrices of the state and measurement noises [22]. In this study, state noise covariance matrix was chosen to be decreased at each iteration due to the decrease in the state modelling error which is one of the components in the state noise. Thus state noise covariance matrix was $\mathbf{Q}_{iteration} = \frac{1}{iteration}\mathbf{I}_2$. Measurement noise covariance matrix was set to a constant small value ($\mathbf{R} = 0.1$) due to the very low noise in the airflow measurements by pneumatograph. Initials were $\theta_0 \sim \mathrm{N}(1,1)$ and $\mathbf{x}_0 = [0.1\ 0.1]^T$ for the model parameter vector and the state vector, respectively.

The next step in the estimation of lung pressures is to optimize the model parameters for the decrease in the state error covariances. At this stage nonlinear optimization problem is given as in (4):

$$\min_{\theta} \sum_{i=1}^{N_{hurst}} \left(y_i - \mathbf{C}\left(\theta\right)\mathbf{x}_i - \mathbf{D}\left(\theta\right)\mathbf{u}_i\right)^2$$
$$\text{s.t.} \quad \mathbf{x}_{i+1} - \mathbf{A}(\theta)\mathbf{x}_i - \mathbf{B}\left(\theta\right)\mathbf{u}_i = \mathbf{0} \quad 1 \le i \le N_{hurst} \tag{4}$$

In this study, interior point optimization method was utilized due to large number of constraints. Detailed explanations can be found in [23]. However, since objective function in this optimization problem is a nonlinear function of the parameters, the solver will likely yield the local minima. In order to avoid suboptimal solutions, we self-iterated optimization solver for 10 runs while randomly choosing the initials. Initial parameters were chosen by $\theta_0 \sim \mathrm{U}(1,10)$ and average of all 10 runs was used as the output of the solver.

E. Feature Calculator

In order to estimate the respiratory parameters, a relevant parameter and its features should be selected somehow. In this work, viscoelastic model parameter R_c which corresponds to the airway resistance was assumed to be related with the respiratory parameters that are measured by clinical tests. Basically, R_c can be obtained by using internal pressures which are rooted back to RSS and measured airflow as given in (5):

$$R_{c,i} = \frac{\hat{P}_{ao,i} - P_{1,i} - P_{2,i}}{Q_i}, \quad 0.3N_{hurst} \le i \le N_{hurst} \tag{5}$$

here $R_{c,i}$ is the time series and only the last $2/3$ part of the pressure signals were used to calculate $R_{c,i}$, because lung pressure estimator needs some time to settle to the actual states. Furthermore, we employed two different statistical features for the size reduction: average power (G_{RC}) and skewness (S_{RC}) of $R_{c,i}$. Basically, average power indicates the total strength of the values of $R_{c,i}$, whereas skewness is the feature which yields the dispersion of the values of $R_{c,i}$ in respect to mean. Both features were selected because they capture global properties of the system, which makes them suitable to correlate with the measured respiratory parameters. Thus for the zero mean time series $R_{c,i}$, the features given in (6) were calculated for all 23 signal sets.

$$G_{RC} = \frac{1}{N_{hurst}} \sum_{i=0.3N_{hurst}}^{N_{hurst}} \left(R_{c,i}\right)^2$$
$$S_{RC} = \frac{\frac{1}{N_{hurst}} \sum_{i=0.3N_{hurst}}^{N_{hurst}} \left(R_{c,i}\right)^3}{\left(\frac{1}{N_{hurst}} \sum_{i=0.3N_{hurst}}^{N_{hurst}} \left(R_{c,i}\right)^2\right)^{3/2}} \tag{6}$$

F. Analyzer

The last step in this work is to relate the calculated features and the respiratory parameters measured by using clinical respiratory function tests. At this stage feature sets of power (G_{RC}) and skewness (S_{RC}) calculated for 19 recordings (due to the lack of lung function tests for the respiratory parameters, recordings 12, 13 and 16, 17 obtained from two subjects were excluded) and respiratory parameter set containing 12 parameters from the remaining 9 subjects were used. Respiratory parameters are given in Table I. In the analysis, basic Pearson correlation coefficient provided the cross correlation between the parameters and features. It was estimated as in (7),

$$\hat{\rho}_{FE,RP} = \frac{\frac{1}{19}\sum_{j=1}^{19} FE_j RP_j}{\left(\frac{1}{19}\sum_{j=1}^{19} FE_j\right)^{1/2}\left(\frac{1}{19}\sum_{j=1}^{19} RP_j\right)^{1/2}} \tag{7}$$

where FE is the feature of either power (G_{RC}) or skewness (S_{RC}), and RP is one of the respiratory parameters explained in Table I. $\hat{\rho}_{FE,RP}$ should be calculated for all respiratory parameters and features, thus 24 correlation coefficient estimates were analyzed.

Pearson correlation coefficient expresses the degree of the linear relationship between the parameters and the features. However it is arguable that the samples of these data sets may not be in the linear relationship, yet the method may be consistent. Therefore, relatively new method which is called Bland-Altman analysis has been used very often in biostatistics

to yield the relationship between the methods or systems that generate different data sets [24]. In this analysis, FE and RP are assumed to be any two of the many data sets and the significant one is difference data (DF), which should be analyzed further. Difference data and related parameters are given in (8)

$$DF_j = FE_j - RP_j \quad 1 \le j \le 19$$
$$m_{DF} = \frac{1}{19}\sum_{j=1}^{19} DF_j$$
$$\sigma_{DF} = \sqrt{\frac{1}{18}\sum_{j=1}^{19}(DF_j - m_{DF})^2} \tag{8}$$

here m_{DF} and σ_{DF} are called as the mean difference data and standard deviation difference data, respectively. In the analysis, Bland-Altman plots were drawn as a scatter plot of difference data versus average data (M) which is given in (9).

$$M_j = \frac{FE_j + RP_j}{2} \quad 1 \le j \le 19 \tag{9}$$

As a summary, data sets are evaluated by incorporating the explanations for the following questions:

- How does the mean difference data m_{DF} change? Does it get high values?
- $m_{DF} \pm 1.96\sigma_{DF}$ is called agreement limits and it is the indication that difference data is in the interval of 95% of the mean in the Gaussian distribution. How data is distributed?
- Is there any limit for the difference data?
- How difference data and average data are related?

III. Results

Hurst exponents time series, which are also called local Hurst exponent values were obtained for all 23 recorded signal sets by using Algorithm 1, $LS1$ and $W_{length} = 512$. How Hurst exponent time series, H_i, $1 \le i \le N_{hurst}$ change in the periods is shown in Fig. 6, which also includes the non-calibrated, decimated and zero mean airflow signal Q_i, $1 \le i \le N_{hurst}$. Positive airflow values are inspiration parts of the breathing. Each figure belongs to different subject and except Record 15 (Fig. 6(c) corresponding to very forceful breathing), results are associated with forceful breathing. These results belonging to $LS1$, are representative results from the whole set. In fact, similar results were obtained for the other RSS. Fig. 7 shows the box-plot representation of the Hurst exponent time series for all 23 recordings. Subject - Recording relations can be seen in the Table II. Subject' box-plot order is first quite and then forceful breathing (e.g. 1,2), apart from subject 2 for who order is quite, forceful and very forceful breathing (3,4,5).

Next, representative results from the output of the mouth pressure estimator are given in Fig. 8, which corresponds to the Hurst exponent time series in Fig. 6. In the figure, non-calibrated and decimated mouth pressure $P_{ao,i}, 1 \le i \le N_{hurst}$ and the estimated mouth pressure $\hat{P}_{ao,i}$, $1 \le i \le N_{hurst}$ are shown in red and in blue plots, respectively. Estimator worked with $LS1$ and $W2 = 512$ window length for all recordings regardless of the least MSE conditions specific to the recording.

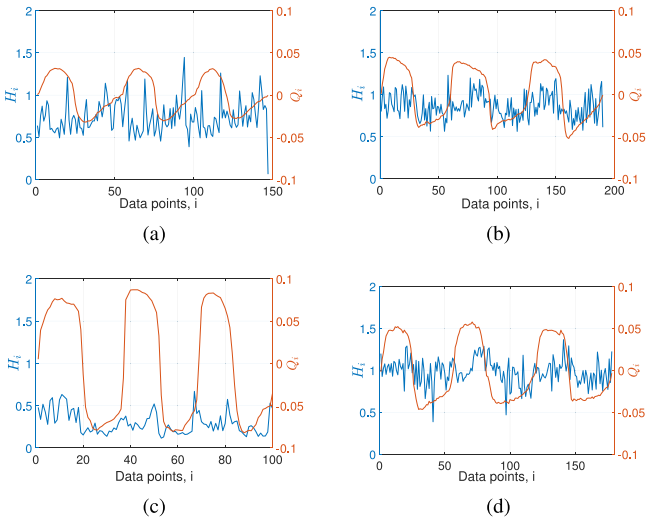

Fig. 6. Hurst exponent time series H_i (calculated by $LS1$ signals), in blue and corresponding airflow signal Q_i, in red, from (a) Record 5 (b) Record 2 (c) Record 15 and (d) Record 9.

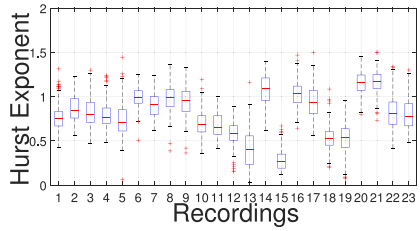

Fig. 7. Box-plot representation of Hurst exponent time series (calculated by $LS1$ signals) for 23 recordings.

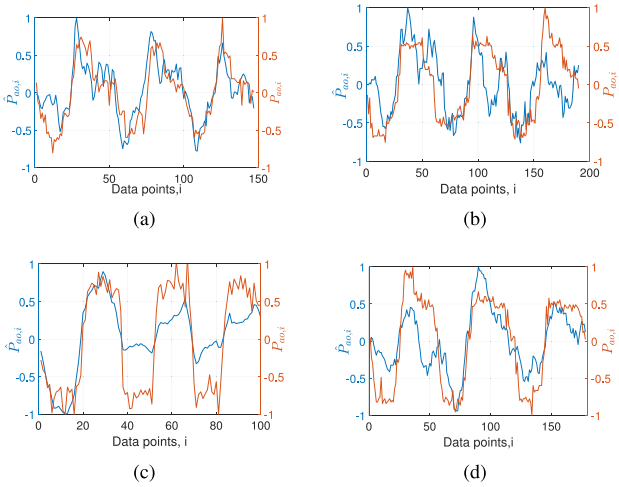

Fig. 8. Estimated mouth pressure $\hat{P}_{ao,i}$, in blue and corresponding measured mouth pressure signal $P_{ao,i}$, in red, from (a) Record 5 (b) Record 2 (c) Record 15 and (d) Record 9.

Fig. 8(a) belongs to Record 5 in which the least MSE was obtained by $LS1$ and $W2 = 512$ window length. However, in Fig. 6(b), (c) and (d), MSE were minimum for $LS1$ and $W4 = 2048$ window length, $LS7$ and $W2 = 512$ window length and $LS3$ and $W4 = 2048$ window length, respectively. MSE values were calculated by (1) are given in Fig. 9 for all recordings.

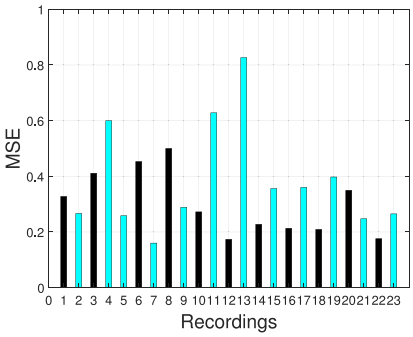

Fig. 9. Bar graphs of MSE values obtained from the mouth pressure estimator for 23 recordings. Black and cyan bars represent quite and forceful breathing conditions respectively.

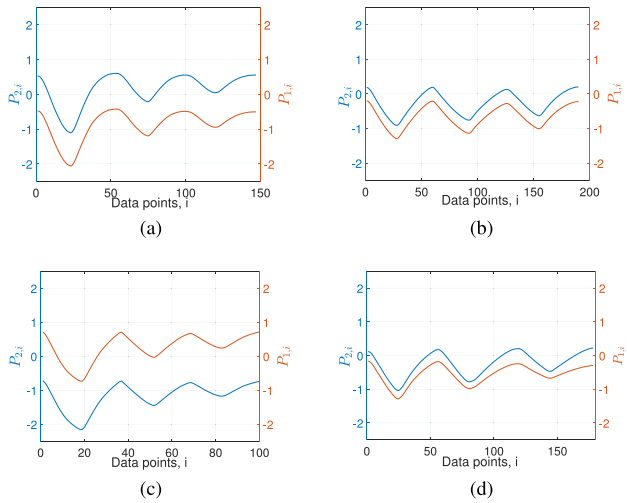

Fig. 10. Estimated internal pressures due to lung static elastance $P_{1,i}$, in red and lung tissue elastance $P_{2,i}$, in blue by using (a) Record 5 (b) Record 2 (c) Record 15 and (d) Record 9.

Comparison between quite breathing and forceful breathing conditions can be done in terms of MSE values in the mouth pressure estimator's performance.

The output of the Part 1 in Fig. 1, which is the estimated mouth pressure was the input of the lung pressure estimator. By adopting the viscoelastic model (Fig. 4) and corresponding state-space equations, (2) and (3), internal pressures related to the lung tissue elastance and static lung elastance were explicitly expressed mathematically for the estimator. Kalman filter together with the interior point optimization solver (Fig. 5) supplied estimation of the pressure signals. Fig. 10 shows estimated internal pressures for the same four recordings shown in both Fig. 6 and Fig. 8.

The output of Part 2 in Fig. 1 is plotted in Fig. 11 for all recordings. The power (G_{RC}) and skewness (S_{RC}) of $R_{c,i}$, $0.3N_{hurst} \leq i \leq N_{hurst}$, found by (6) are shown in Fig. 11(a) and Fig. 11(b), respectively.

The last results which are the outcomes from the analyzer (Part 3 in Fig. 1) are shown in Fig. 12. Fig. 12(a) and (b) depict the correlation coefficients between the power and skewness features and all twelve respiratory parameters calculated by (7), respectively. It is observed that feature power and respiratory

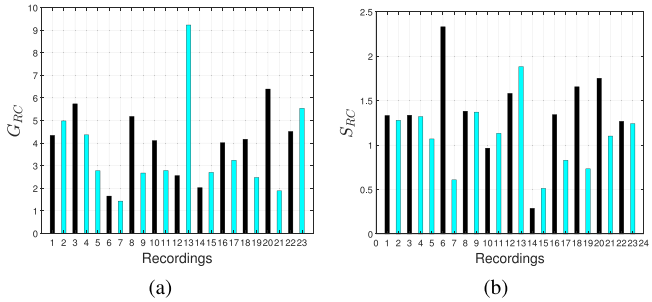

Fig. 11. Features (a) average power (G_{RC}) and (b) skewness (S_{RC}) of $R_{c,i}$, $0.3N_{hurst} \leq i \leq N_{hurst}$, obtained for 23 recordings.

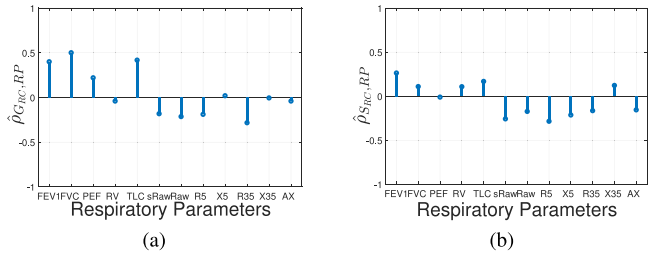

Fig. 12. Correlation coefficient between (a) respiratory parameters and average power (G_{RC}) and (b) respiratory parameters and skewness (S_{RC}).

parameter FVC are positively correlated with correlation coefficient of 0.5 ($p < 0.05$). Feature power and FEV1 and TLC are also positively correlated with significant statistics ($p < 0.10$), but the rest of the relationships are not significant. On the other hand, there is no significant relationship between feature skewness and any respiratory parameter.

Bland-Altman plots which are drawn by using feature power (FE is G_{RC}) and feature skewness (FE is S_{RC}) are given in Fig. 13 and in Fig. 14, respectively. In the figures, subplot titles correspond to one of the Respiratory Parameters given in Table I and Bland-Altman plot of that parameter is given in the subplot. In order to compare the plots, axes limits are set to the same range. In the plots, upper blue and lower magenta lines are the agreement limits in which most of the data are located. Mean difference data (m_{DF}) is shown as green line in the middle. How the data are distributed in the plots can be inspected by the linear regression line which is shown as a dotted red line.[1]

IV. Discussion

DFA method has the ability to illustrate structural similarities hidden in the signals by removing trends. Since RSS and RS contain slowly changing trends, DFA provided useful estimate of the parameter Hurst exponent, H, in order to elaborate the fractal properties of RSS and RS. In this study, direct application of Algorithm 1 alone provided the exponents. How Hurst exponents evolve in three periods of $LS1$ can be seen in Fig. 6. First it is noticeable that Hurst exponent time series have noisy trends. It increases in inspiration and decreases in expiration. However for three recordings (one of them is shown in Fig. 6(a)) Hurst

[1]Matlab programs of the simulations are provided at https://github.com/EsraSaatci/Respir-Para-Estim

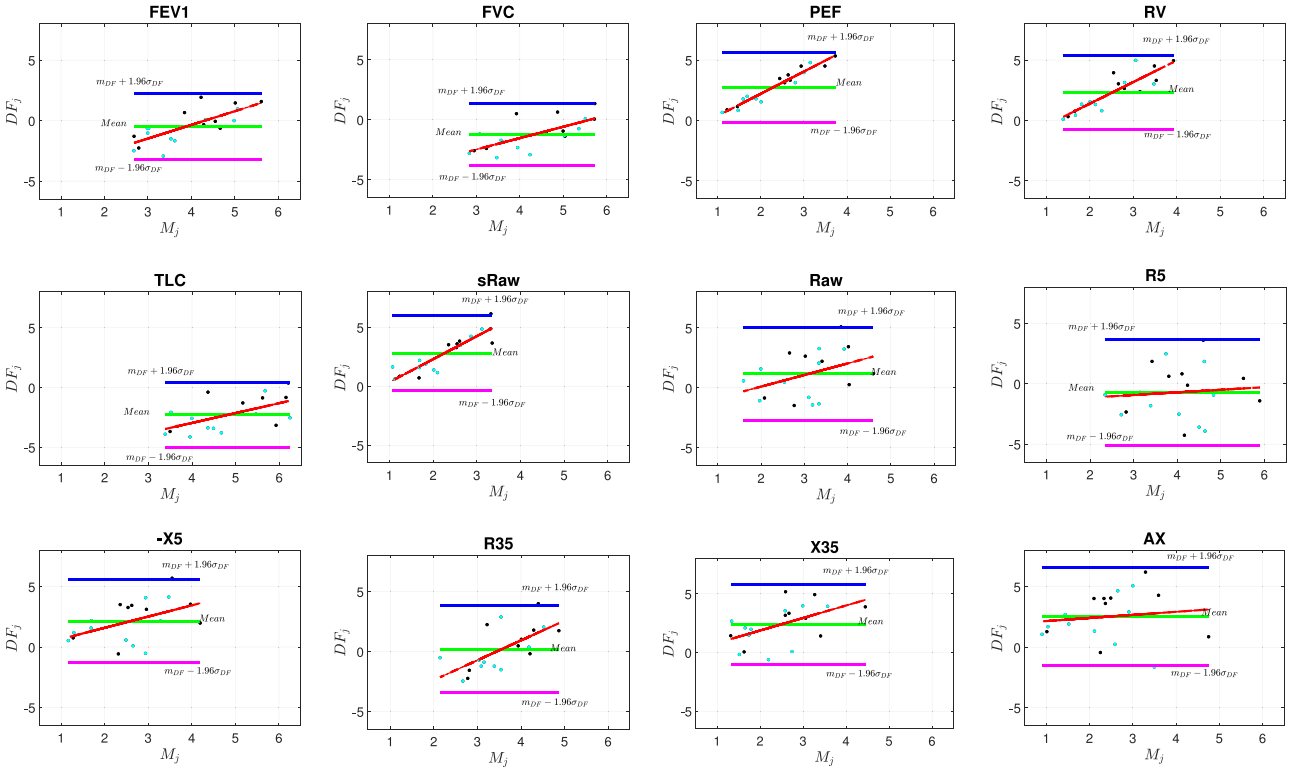

Fig. 13. Bland-Altman plots for feature power (FE) paired with all measured Respiratory Parameters (RP is one of the Respiratory Parameters given in Table I) are given in the subplots for 19 calculated values ($1 \leq j \leq 19$). Black and cyan dots represent quite and forceful breathings respectively.

exponent values follow inspiration and expiration with a lag. This should be investigated further by increasing the number of the recordings and explaining the statistical properties of RSS. Furthermore, the correlation between the signals emerged from the dynamics in the respiratory system and RSS should be evaluated thoroughly.

In this study, as we explained above, Hurst exponent time series are merely utilized to estimate the mouth pressure and internal pressures. On the other hand, valuable physiological explanations can be made in Fig. 7 where all results are shown by box-plots. First of all, it is observed that Hurst exponent changes inside a period, thus they are local H values, which is another way to demonstrate that $LS1$ is a multifractal signal. In fact, this is also correct for other RSS. This result is matched with the results presented in [15] where multifractal evaluation were performed on RS and RSS. Medians for all recordings depend on the subject whereas effective ranges, which are the length of the boxes, are approximately the same in the recordings. Apart from the subject 5 (recordings 12 and 13) and the subject 6 (recordings 14 and 15), Hurst exponent medians and ranges are the same in quite and forceful breathing. Considerable amounts of Hurst exponent values are between 0.5 and 1, there is one major explanation for this situation, that is $LS1$ or generally RSS is the fractional Gaussian noise type signal with persistent behavior, which means increasing trend or decreasing trend can be seen in RSS.

When we evaluate the mouth pressure estimation by RLS, it is obvious in Fig. 8 that the performance of the estimator is sufficiently high even if MSE parameters employed in the estimator were not the least MSE parameters. Estimator output successfully tracked three periods of the mouth pressure. This is a good indication that there is no need to use pressure sensor, thus, this method can be employed to mimic mouth pressure in the analyses. Since the mouth pressure is available, efficiency of the estimator can be judged directly from the figures. However, more interesting and informative results are obtained from Fig. 10 where internal pressure estimates can be seen.

First of all, it is seen that Kalman filter resulted in smooth and filtered pressures. This is because Gaussian noise is filtered out by correctly chosen error covariance matrices. Due to the page limits, we did not present the results for all 23 recordings. However, those four plots in Fig. 10 represent all set very well. We obtained similar internal pressure results as in Fig. 10(a), (b) and d for all quite and forceful breathing, but for the record 15 (in Fig. 10(c)) and record 13 (not shown) plots have one very important difference, that is lung static elastance $P_{1,i}$ is higher than lung tissue elastance $P_{2,i}$. It is very difficult to explain this issue physiologically, because to the best of our knowledge there is no study for the comparison of the internal pressures in this set-up by using signals. In [7] and [25] viscoelastic properties of the lung was examined by experimental set-up in static conditions and under mechanical ventilation for the non-healthy lungs. In these studies viscoelastic model and its variants were used to estimate the parameters. According to the results, static elastance was found to be less than viscoelastic elastance of the model. Thus our study is a new interpretation of the viscoelasticity of the respiratory system which reveals consistent outcomes with the previous work. Furthermore, it can be easily seen that for the

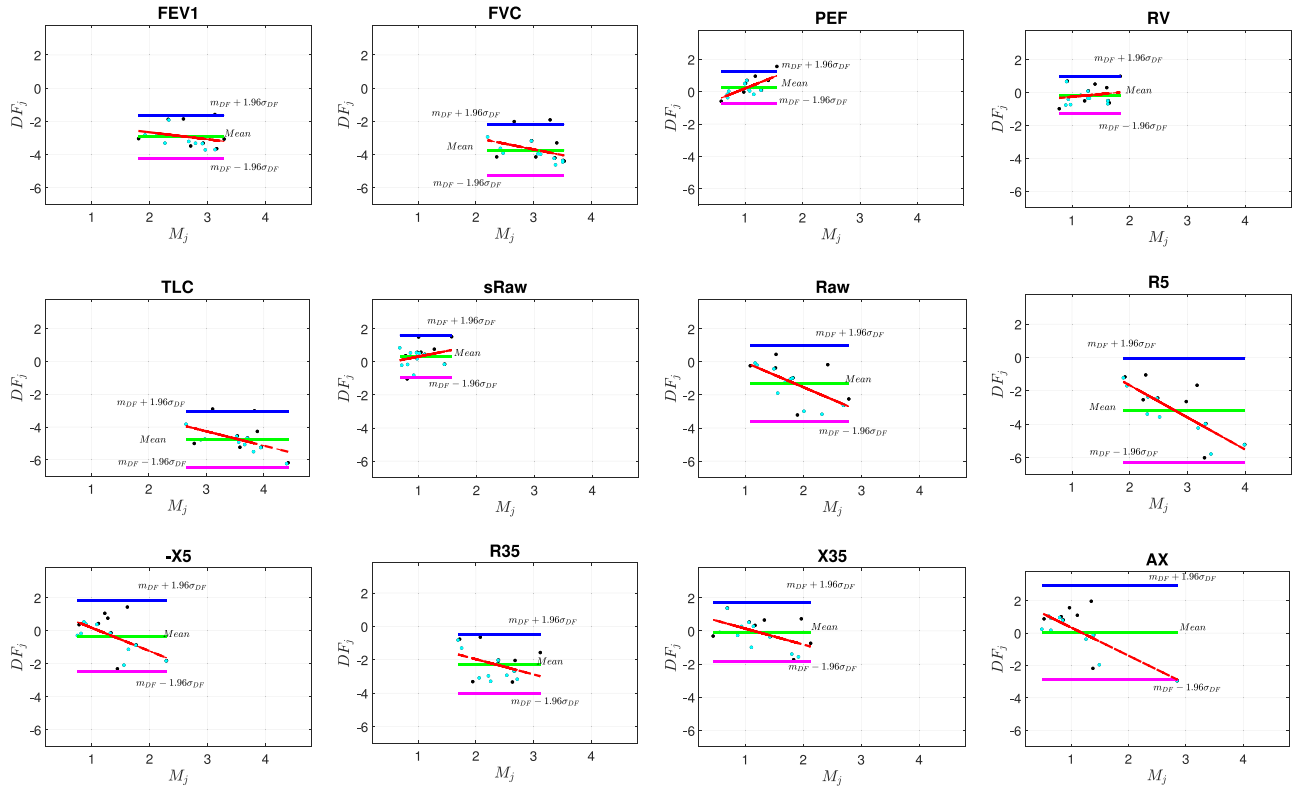

Fig. 14. Bland-Altman plots for feature skewness (FE) paired with all measured Respiratory Parameters (RP is one of the Respiratory Parameters given in Table I) are given in the subplots for 19 calculated values ($1 \leq j \leq 19$). Black and cyan dots represent quite and forceful breathings respectively.

record 13 and 15 medians of Hurst exponents are below 0.5, so $LS1$ shows antipersistant behavior (increase will most likely be followed by the decrease and vice versa). Statistical property of $LS1$ may affect the estimation.

Features, G_{RC} and S_{RC} in Fig. 11 belong to chosen model parameter $R_{c,i}, 0.3N_{hurst} \leq i \leq N_{hurst}$, thus, before interpreting the results we should comment on the expected outcomes. First of all, chosen model parameter corresponds to the airway resistance, so we expect to see a change around mean value in the transition of inspiration to expiration and vice versa. Since the change should have a moderate speed (neither instantaneous nor very slow change), low value to high value or high value to low value change should be gradual making the values positive or negative skewed depending on the density of the specific $R_{c,i}$. If the power feature is integrated to this scenario, one can reveal whether low or high values dominates the range of $R_{c,i}$. There is no normal or expected value for the power feature, therefore it is only used for the comparison.

In this respect, when Fig. 11(a) is analyzed, following observations can be made: *i)* Various power feature values characterized by the subjects can be recognized, *ii)* There are one very high power feature value (recording 13), many middle range powers and three low power feature values (recordings 6, 7 and 21), *iii)* Power feature values are lower in the forceful breathing than in the quite breathing for 7 subjects, but for 3 subjects (subjects 1, 7 and 11) a slight increase exists and for one subject (subject 6) there is an increase. Final remark clearly indicates that forceful breathing decreased the average power of the estimated model parameter $R_{c,i}$ in the most of the subjects. This is mainly due to the increase in the airflow in the healthy subjects.

Skewness feature values in Fig. 11(b) are all positive indicating that $R_{c,i}$ values are left skewed. Most of $R_{c,i}$ values are concentrated on the left of the mean, that is high numbers of small values exist and values are slowly increased. This feature is less evident for six recordings (recordings 7, 10, 14, 15, 17, 19) in which skewness is lower than 1. Therefore, low values of $R_{c,i}$ dominates the time series of $R_{c,i}$.

Last but not least, how features are linearly related to the measured respiratory parameters are given in Fig. 12. Unfortunately, correlation coefficients do not provide meaningful results. According to the figures, only feature power and respiratory parameters of TLC, FEV1 and FVC have statistically significant positive linear correlation. It is interesting that FVC and FEV1 parameters were obtained from the spirometric tests and TLC was measured by the plethysmographic test. Moreover, they are related to the lung volume and airflow measurements. However, non-existence of strong linear association does not mean that two systems are not related and outputs are not correlated. Thus, the link between the features and clinically measured respiratory parameters can be scrutinized in descriptive way via Bland-Altman plots.

Analysis of Bland-Altman plots shown in Fig. 13 and Fig. 14

- Mean difference data (m_{DF}) takes different values in the subplots. Feature power resulted in zero mean difference for respiratory parameters of FEV1 and R35, whereas zero mean difference were obtained for feature skewness and

respiratory parameters of PEF, RV, sRaw, -X5, X35 and AX. This results can be interpreted as respiratory parameters measured by Impulse Oscillometry is more compatible with the feature skewness than the feature power. Apart from those plots mentioned above, the rest of the mean differences were biased, lying above or below zero.

- Zero mean difference is included in the agreement limits in all plots when feature power is used. On the other hand, only for PEF, RV, sRaw, Raw, -X5, X35 and AX agreement limits cover zero mean difference. Zero mean difference line yields the equality between the features and the respiratory parameters, thus if the agreement limits include the equality line, it is said that systems have statistically significant similarity. One can easily conclude that feature power provides results which are compatible with all respiratory parameters.
- We can observe that most of the data are in between the agreement limits. It means that agreement limits provide confidence intervals based on *a piori* limits of maximum acceptable differences.
- Differences between feature power and all respiratory parameters, except R5 and AX have positive trends with respect to the mean of the data sets. It can be easily observed by the linear fit (dotted red line in the figures). It is called as a proportional bias and indicates that two data sets (feature and respiratory parameter sets for 19 recordings) are in agreement which depends on the values in the data sets. This is very obvious for plots where feature power paired with respiratory parameter PEF and sRaw and feature skewness paired with respiratory parameter PEF and RV.
- Data distributed evenly in between the agreement limits for the plots of feature power paired with R5 and AX and feature skewness paired with FEV1 and RV. In this case, linear fit line has very low slope indicating that two data sets have random differences. Randomness in the mean difference should be scrutinized further in order to asses the agreement between the methods.
- If we only evaluate resistance related parameters, feature power is in good agreement with sRaw, because mean difference can be predicted by the mean of the data sets. However due to random difference, feature power is not the best candidate to estimate R5, Raw and R35. If feature skewness paired with resistance related respiratory parameters (sRaw, Raw, R5 and R35), we can observe proportional bias which indicates a more orderly agreement between the data sets.

V. Conclusion

This study purposes a combination of methods to estimate the clinically useful respiratory parameters by involving minimum number of RS and RSS. That requires configuring the processing of RS and RSS from the raw signal to the meaningful features. Overall proposed method includes mainly fractal and statistical signal processing tools to utilize the different aspects of the signal features. In this study, carefully designing each step of the proposed method yielded successful results and at the end, validation results provided a strong link between the raw signals and the features. Main contributions of this work are:

- Fractal properties especially Hurst exponent of the RSS are fruitful representation of the signals which brings the underlying system characteristics into the surface. It was shown that Hurst exponent, itself, can be used as a new tool to reveal the inter-subject variations.
- On the way to the portable respiratory tests, this study developed very important steps. Mouth pressure and internal pressures were estimated successfully by using only RSS. However, it should be recollected that estimated pressures resemble the measured pressures in the respiratory system which can be used in the determination of the respiratory parameters.
- In this study, viscoelastic model parameter of airway resistance was chosen as a representative parameter and features were determined based on the characteristics of the airway resistance such as the increasing and decreasing values in the interval. It is shown that selected features provided distinctive results for 23 recordings.
- Bland-Altman plots were very successful in demonstrating the connection between the two data sets. Validation of the computed features with respect to the clinically measured respiratory parameters proved that proposed method is solid to be used to estimate the clinically useful parameters.
- This study is a pilot study which provides an evidence for the potential use of the link between RS and RSS properties and clinically measured parameters. First of all, in the proposed general framework, each part of this study can be analysed and extended further to include different clinical settings, classified results and conclusions. However, our main results in Fig. 13 and Fig. 14 justify the soundness of the overall method by supporting the proposal that there is a good consistency between the extracted features and some of the clinically critical parameters. Finally, in this study we also aimed to utilize the minimum number of the signals (i.e. sensors) so that proposed parts can be ported to the mobile devices easily and efficiently in the future studies. Therefore, eliminating the need of the pressure sensor by estimating the mouth pressure from the respiratory sounds, determining the proper feature and clinical parameter pair, and facilitating the optimized algorithm will eventually lead us to the ultimate contribution of this work.

Appendix
Multifractal Detrended Fluctuation Analysis

If N sample signal, $x(n)$, is one of RSS assumed to be Gaussian noise like signal, the profile Y_i is computed by integrating the mean reduced signals as:

$$Y_i = \sum_{n=1}^{i} [x(n) - \langle x \rangle] \tag{10}$$

here $\langle x \rangle$ is the mean of $x(n)$ and $i = 1, \ldots, N$.

Starting from the first and then the last samples, Y_i is divided into non-overlapped intervals equal to time scale of length $s \in Z^+$ by a rectangular window. At the end, we have segments $Y_v(i)$ of Y_i, $v = 1, \ldots, 2N_s$ ($N_s \equiv \text{int}(N/s)$).

Local trend for each segment, which is shown by mth order polynomial $y_v(i)$ is computed by least square fit and mean squares fluctuations between the segment and its polynomial fit is computed as:

$$F^2(v,s) = \frac{1}{s}\sum_{i=1}^{s}\left[Y_v(i) - y_v(i)\right]^2 \tag{11}$$

Second order fluctuation function $F_2(s)$ is calculated for the set of time scale values as:

$$F_2(s) = \left\{\frac{1}{2N_s}\sum_{v=1}^{2N_s} F^2(v,s)\right\}^{1/2} \tag{12}$$

and finally if the original signal $x(n)$ is long range correlated, power law relationship shown as:

$$F_2(s) \propto s^H \tag{13}$$

and logarithm function are used to compute the Hurst exponent H. Details and considerations of above algorithm were given in [17].

ACKNOWLEDGMENT

The Study has ethical approval from Ethical Committee of Istanbul Kultur University, (2018.01 and dated 1, April 2018).

REFERENCES

[1] H. Smith, P. Reinhold, M. Goldman, "Forced oscillation technique and impulse oscillometry," *Eur. Respir. Monograph*, vol. 31, pp. 72–105, 2005.
[2] J. H. T. Bates *et al.*, "Lung tissue rheology and 1/f noise," *Ann. Biomed. Eng.*, vol. 22, pp. 674–681, 1994.
[3] C. Ionescu *et al.*, "Low frequency constant-phase behavior in the respiratory impedance," *Biomed. Sig. Process.*, vol. 6, pp. 197–208, 2011.
[4] C. Ionescu, J. A. T. Machado, R. De Keyser, "Modeling of the lung impedance using a fractional-order ladder network with constant phase elements," *IEEE Trans. Biomed. Eng.*, vol. 5, no. 1, pp. 83–89, Feb. 2011.
[5] J. H. T. Bates, *Lung Mechanics*, Cambridge, U.K.: Cambridge Univ. Press, 2009.
[6] E. Saatci, E. Saatci, A. Akan, "Analysis of linear lung models based on state-space models," *Com. Methods. Prog. Biomed.*, vol. 183, pp. 1–9, 2020.
[7] Z. Dai *et al.*, "A model of lung parenchyma stress relaxation using fractional viscoelasticity," *Med. Eng. Phys.*, vol. 37, no. 8, pp. 752–758, 2015.
[8] L. J. Hadjileontiadis and S. M. Panas, "A wavelet-based reduction of heart sound noise from lung sounds," *Int. J. Med. Inf.*, vol. 52, no. 1, pp. 183–190, 1998.
[9] Z. K. Moussavi, "Fundamentals of Respiratory Sounds and Analysis," Synthesis Lectures on Biomedical Engineering, Morgan Claypool, vol. 1, no. 1, pp. 1–68, 2006.
[10] A. Mondal, P. Banerjee, H. Tang, "A novel feature extraction technique for pulmonary sound analysis based on EMD," *Com. Methods. Prog. Biomed.*, vol. 159, pp. 199–209,2018.
[11] V. K. Iyer, P. A. Ramamoorthy, H. Fan, and Y. Ploysongsang, "Reduction of heart sounds from lung sounds by adaptive filtering," *IEEE Trans. Biomed. Eng.*, vol. BME-33, no. 12, pp. 1141–1148, Dec. 1986.
[12] N. Reljin, B. A. Reyes, and K. H. Chon, "Tidal volume estimation using the blanket fractal dimension of the tracheal sounds acquired by smartphone," *Sensors*, vol. 15, pp. 9773–9790, 2015.
[13] C. M. Ionescu, W. Kosinski, and R. De Keyser, "Viscoelasticity and fractal structure in a model of human lungs," *Arch. Mech.*, vol. 62, no. 1, pp. 21–48, 2010.
[14] M. Costa, A. L. Goldberger, and C. K. Peng, "Multiscale entropy analysis of biological signals," *Phys. Rev.*, vol. 71, no. 2, 2005, Art. no. 021906.
[15] E. Saatci and E. Saatci, "Multifractal behavior of respiratory signals," *Electrica*, vol. 20, no. 2, pp. 182–188, 2020.
[16] J. W. Kantelhardt *et al.*, "Multifractal detrended fluctuation analysis of nonstationary time series," *Physica A*, vol. 316, pp. 87–114, 2002.
[17] E. A. f. Ihlen, "Introduction to multifractal detrended fluctuation analysis in matlab," *Front. Physiol*, vol. 3, no. 141, pp. 1–18, 2012.
[18] Z. K. Moussavi *et al.*, "Computerised acoustical respiratory phase detection without airflow measurement," *Med. Biol. Eng. Comp.*, vol. 38, pp. 198–203, 2000.
[19] E. Perrin *et al.*, "nth-order fractional brownian motion and fractional gaussian noises," *IEEE Trans. Sig. Process.*, vol. 49, no. 5, pp. 1049–1059, May 2001.
[20] S. Haykin, *Adaptive Filter Theory*, 5th ed., London, U.K.: Pearson, 2013.
[21] M. S. Grewal, A. P. Andrews, *Kalman Filtering*, Hoboken, NJ, USA: Wiley, 2001.
[22] M. R. Ananthasayanam *et al.*, "A heuristic reference recursive recipe for adaptively tuning the kalman filter statistics Part-1: Formulation and simulation studies," *Sadhana*, vol. 41, no. 12, pp. 1473–1490, 2016.
[23] A. Wachter and L. T. Biegler, "On the implementation of an interior point filter line-search algorithm for large-scale nonlinear programming," *Math. Prog.*, vol. 106, pp. 25–57, 2006.
[24] D. Giavarina, "Understanding bland altman analysis," *Biochemia Medica*, vol. 25, no. 2, pp. 141–51, 2015.
[25] V. Antonaglia *et al.*, "Single-breath method for assessing the viscoelastic properties of the respiratory system," *Eur. Respir. J.*, vol. 12, pp. 1191–1196, 1998.